Transport Modeling for Nanoscale Semiconductor Devices

(Invited Paper)

M. Pourfath, V. Sverdlov, and S. Selberherr
Institute for Microelectronics, TU Wien, 1040 Vienna, Austria
Email: {pourfath|sverdlov|selberherr}@iue.tuwien.ac.at

***Abstract*— Due to extreme miniaturization of device dimensions the well established TCAD tools are pushed to the limits of their applicability. Since conventional MOSFETs are already operating in the sub-100 nm range, new physical effects and principles begin to determine the transport characteristics and the validity of conventional current transport models is in question. The classical drift-diffusion model of carrier transport in electronic devices has been widely employed in TCAD tools. However, it must be generalized to include hot-carrier effects. This motivated the development of higher-order moments transport models such as the hydrodynamic transport model, the energy transport model, and the six-moments model. With scaling continuing quantum mechanical effects begin to affect the transport properties. Parallel to the search for new technological solutions for MOSFET scaling, the development of conceptually new devices and architectures is becoming increasingly important. New nanoelectronic structures, such as carbon nanotubes, nanowires, and even molecules, are considered to be prominent candidates for the post-CMOS era. At this small device size the geometrical spread of the carrier wave packet in transport direction can no longer be ignored. When the device size becomes shorter than the coherence length, the complete information about the carrier dynamics inside the device including the phase of the wave function is needed and one has to resort to a full quantum mechanical description including scattering. Transport in advanced nanodevices is determined by the interplay between coherent propagation and scattering. Numerical methods for dissipative quantum transport based on the non-equilibrium Green's function formalism, the Liouville/von-Neumann equation for the density matrix, and the kinetic equation for the Wigner function are attaining relevance. In this work we review semi-classical and quantum mechanical modeling of carrier transport in nanoscale semiconductor devices.**

1. Introduction

For more than four decades the progress of integrated circuit technology has been based upon the down-scaling of Si MOSFETs. The number of devices contained on a single chip has approximately doubled every three years. The continued miniaturization of Si integrated devices has approached the deca nanometer region. Novel structures, such as multiple gate MOSFETs, and novel materials beyond Si, such as graphene, are expected to be utilized to meet the requirements for further scaling [1]. Rapid changes in technological solutions and device architectures can be anticipated by employing technology computer-aided design (TCAD) tools which assist in device development and engineering at practically all stages from process definition to circuit optimization.

The classical drift-diffusion model of carrier transport in electronic device has been widely employed in TCAD tools. From an engineering point of view, semi-classical models, such as the drift-diffusion transport model, have enjoyed an amazing success due to their relative simplicity, numerical robustness, and the ability to perform two- and three-dimensional simulations on large unstructured meshes [2]. However, with device size dramatically reduced TCAD tools based on semi-classical transport description begin to show shortcomings. The problem is two-fold. First, with the downscaling the driving field and its gradient increase dramatically in short channels. As a result the carrier distribution along the channel can no longer be described by the shifted and heated Maxwellian distribution. In order to properly account for hot-carrier and non-local effects, the drift-diffusion and even the energy transport model have to be improved to incorporate the substantial modifications in the distribution function. The second, more fundamental reason for semi-classical modeling tools to gradually loose their validity lies in the particle-wave duality of carriers. When the device dimensions are comparable to the carrier wave length, the carriers can no longer be treated as classical point-like particles, and effects originating from the quantum mechanical nature of propagation begin to determine transport.

In Sec. 2 semi-classical transport models are briefly introduced and full-band Monte Carlo simulation results for strained Si are presented. In Sec. 3 quantum transport models are discussed in moderate detail and the role of line-edge roughness in graphene nanoribbons (GNRs) is investigated. Finally, conclusions are drawn in Sec. 4.

2. Semi-classical Transport Models

Table I sketches the hierarchy of different transport models for device modeling. There are two fundamental equations for semi-classical device simulation, the Poisson equation and the Boltzmann equation. While

978-1-4244-5799-1/10/$26.00 ©2010 IEEE

TABLE I
The hierarchy of semi-classical and quantum transport models.

Transport Regime	Semi-classical $L \gg \lambda, \ell$				Quantum Mechanical $L \sim \lambda, \ell$	
Fundamental Equation	Boltzmann				Schrödinger	
Transport Model	Drift-Diffusion	Hydrodynamics	Boltzmann (Monte Carlo)	Quantum Corrected Boltzmann Quantum Hydrodynamics	Wigner	Non-equlibrium Green's Function

Device Scaling →

the Poisson equation takes care of the electrostatic description of any device structure, the Boltzmann equation describes the propagation of particles with a distribution function $f(\mathbf{r}, \mathbf{k}, t)$ in the device. These two equations have to be solved in a self-consistent manner and can be exploited as a reference for numerous models which are derived from the Boltzmann transport equation [3]. The distribution function $f(\mathbf{r}, \mathbf{k}, t)$ is a classical concept which holds, when the characteristic length of the device is much larger than the De Broglie wavelength, $L \gg \lambda$, and the mean free path of carriers, $L \gg \ell$.

A direct solution of the Boltzmann equation is possible only for a few rather special cases. In general the Boltzmann equation can be numerically solved by using the Monte Carlo method [4]. An approximate solution can be obtained by expressing the distribution function as a series expansion which leads to the spherical harmonics approach [5].

The method of moments is also a very efficient way to derive approximate solutions of the Boltzmann transport equation [3]. By multiplying the Boltzmann transport equation with a set of weight functions and integrating over k-space one can deduce a set of balance and flux equations coupled with the Poisson equation. Via this formalism an infinite chain of coupled equations can be generated. One has to truncate the equation system at a certain point and complete the system by introducing an additional condition [6]. For example, the drift-diffusion model can be gained by assuming thermal equilibrium between the charge carriers and the lattice [3]. However, when the device size is scaled down, the carriers' non-equilibrium properties caused by a high electric field become important. The hydrodynamic transport model addresses this issue by assuming a heated Maxwellian distribution for the carriers [7].

2.1. Application to Strained Si

In the mid 1970's a physical model of Si has been developed, capable of explaining major macroscopic transport characteristics [8, 9]. The used band-structure models were represented by simple analytical expressions accounting for non-parabolicity and anisotropicity. With the increase of the carriers' energy the need for accurate, numerical energy band-structure models arose [10]. For electrons in Si, the most thoroughly investigated case, it is believed that a satisfactory understanding of the basic scattering mechanisms gives rise to a new "standard model" [11]. With the introduction of strain to enhance the performance of MOSFETs, however, the need for accurate full-band transport analysis has regained considerable interest [12, 13].

Fig. 1 shows simulation results for the electron mobility of strained Si for the stress directions $[100]$ and $[110]$ as well as predictions from a model based on the linear piezoresistance coefficients [14]. Mobility is plotted in three directions, one being parallel and two being perpendicular to stress.

In Fig. 1(a) the results from analytical band and full-band Monte Carlo simulations for stress along $[100]$ are compared and good agreement is obtained. The resulting mobility is anisotropic in the (001) plane ($\mu_{[100]} \neq \mu_{[010]}$), and can be explained by strain induced X-valley shifts [15]. Mobility saturates at approximately 1% strain, regardless of the sign of strain. The saturated mobility values are larger for compressive strain, since in this case four X-valleys with unfavorable conductivity masses are depopulated [15].

In Fig. 1(b) simulation results are shown for stress along $[110]$. For tensile stress along $[110]$, the mobility behavior is remarkably different from the previous case. First, mobilities along the directions $[110]$, $[\bar{1}10]$, and $[001]$ are different from each other, with the largest mobility enhancement observed in $[110]$ direction. Furthermore, no clear in-plane mobility saturation is observed as stress increases. The mobility enhancement for tensile stress is determined by the effective mass change induced by the shear strain component in the primarily populated valleys along $[001]$ [15, 16].

It can be seen that the results from analytical band and full-band Monte Carlo simulations agree well up to 0.5% shear strain. At larger strain levels the band deformation is so pronounced that the energy band description in terms of an effective mass is no longer accurate, and full-band Monte Carlo simulations must be used even for the calculation of the low-field mobility.

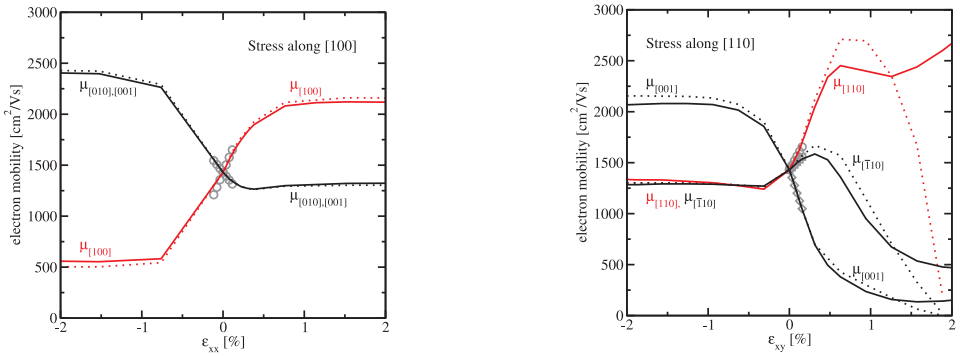

(a) (b)

Fig. 1. Simulated bulk mobility of intrinsic Si as a function of strain for stress direction [100] (a) and [110] (b). Mobility is plotted along the stress direction and along two orthogonal directions from full-band Monte Carlo simulations (solid lines) and analytical band Monte Carlo simulations (dotted lines). Symbols indicate the change of mobility calculated using the piezoresistance coefficients [14].

3. Quantum Mechanical Transport Models

The Poisson equation and the Schrödinger equation are the basis of all quantum transport models. However, solving the Schrödinger equation for a many particle system is very difficult. To address this problem different techniques and methods have been introduced. Among them the non-equilibrium Green's function (NEGF) formalism appears to be appropriate for nanoscale devices [17, 18]. This method has been successfully applied to study molecular devices [19–21], Si MOSFETs [22–25], nanowires [26–29] CNTs [30–34], GNRs [35–38], and spin transport [39–41]

In coordinate representation the Green's function, $G(\mathbf{r_1}, t_1; \mathbf{r_2}, t_2)$, depends on two position arguments $\mathbf{r_1}, \mathbf{r_2}$ and two time arguments t_1, t_2, representing the non-locality in space and time. Under steady state condition the Green's functions depend only on time differences. One usually Fourier transforms the time difference coordinate, $\tau = t_1 - t_2$, to energy $G(\mathbf{r_1}, \mathbf{r_2}; E) = \int (d\tau/\hbar) e^{iE\tau/\hbar} G(\mathbf{r_1}, \mathbf{r_2}; \tau)$.

The equation of motion for the Green's function is given by the integro-differential Dyson equation [42]. Starting from the Dyson equation, the quantum Boltzmann equation can be derived [43]. When independent variables are changed to the center of mass coordinates $(\mathbf{r}, t) = (\mathbf{r}_1 + \mathbf{r}_2, t_1 + t_2)/2$ and the relative coordinates $(\mathbf{u}, \tau) = (\mathbf{r}_1 - \mathbf{r}_2, t_1 - t_2)$, a quantum mechanical distribution function $G(\mathbf{k}, \omega, \mathbf{r}, t)$ is defined as the Fourier transform of $G(\mathbf{u}, \tau, \mathbf{r}, t)$ with respect to the relative coordinates. The quantum Boltzmann equation is in fact a kinetic differential equation for the Green's function $G(\mathbf{k}, \omega, \mathbf{r}, t)$ [43].

The Wigner distribution function is defined as the energy integral of the Green's function, $f(\mathbf{k}, \mathbf{r}, t) = \int G(\mathbf{k}, \omega, \mathbf{r}, t) d\omega$ [44]. A transport equation for the Wigner distribution function including scattering effects can be obtained [45]. A practically used approximation to incorporate realistic scattering processes into the Wigner equation is to utilize the Boltzmann scattering operator [46], or by an even simpler scheme such as the relaxation time approximation[47]. Under this approximation, quantum mechanical collisional effects, for example, collisional energy broadening [48], are neglected. One can rewrite the Wigner equation in the form of a modified Boltzmann equation with additional terms including quantum correction [44]. Based on this equation the quantum corrected Boltzmann equation, the quantum hydrodynamic approximation, and the density gradient approximation can be devised [49].

3.1. Analysis of Graphene Nanoribbons

Graphene, a one-atomic carbon sheet with a honeycomb structure, has attracted significant attention due to its unique physical properties [50]. This material shows an extraordinarily high carrier mobility of more than $2 \times 10^5 \mathrm{cm}^2/\mathrm{Vs}$ [51] and is considered a major candidate for a future channel material for high performance transistors [52, 53]. To induce an electronic bandgap, a graphene sheet can be patterned into narrow ribbons [54]. In order to obtain an energy bandgap larger than $0.1\mathrm{eV}$, which is essential for electronic applications, the width of the GNR must be scaled below $10\mathrm{nm}$ [55]. In this regime line-edge roughness is the dominant scattering mechanism [56]. Applying an atomistic tight-binding model [54] and the NEGF method the effect of line-edge roughness in GNRs is studied. Employing an atomistic tight-binding model one can capture the granularity of the simulation domain, which is essential for narrow GNRs.

The line-edge roughness can be perturbatively treated [56]. However, in a more accurate non-perturbative approach one can consider the roughness as a stochastic phenomenon and adapt it by removing or

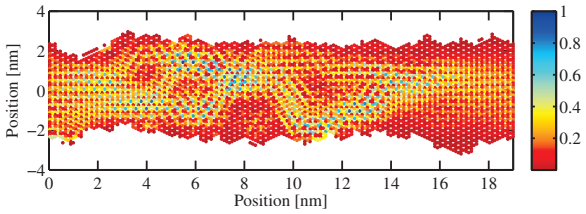

Fig. 2. Spatial distribution of the normalized current amplitude along a GNR with line-edge roughness. The ribbon's length is 19nm and the width is 5nm. The roughness is described by a correlation length of $L_m = 3\text{nm}$ and an amplitude of $\Delta_m = 2a_{cc}$.

replacing specific carbon atoms located at the edges of the ribbon. In order to model roughness, an exponential auto-correlation function is defined as [57]:

$$c(n) = \Delta_m^2 \exp\left(-\frac{x}{L_m}\right), \quad x = n\Delta x \qquad (1)$$

Δ_m is the roughness amplitude, L_m is the correlation length, and $\Delta x = a_{cc}/2$ is the sampling interval. The stochastic roughness can be generated by applying a random phase to the power spectrum of the roughness auto-correlation in the Fourier domain and inverse Fourier transforming in order to obtain roughness in the real space domain [57]. Fig. 2 shows the spatial distribution of the current amplitude along a GNR with rough edges. Localization of carriers can be seen along the ribbon. In case of strong localization, carriers tunnel from one localized state to another one. In this regime the resistance of the device increases exponentially with its length [48]. However, with the aid of these analyses one can obtain the required geometrical and roughness parameters to avoid this phenomena in electronic devices.

4. Conclusion

A review of semi-classical and quantum mechanical transport models for the analysis of semiconductor devices is presented. The approximations and the limitations of each model are discussed. As a case study full-band Monte Carlo simulation results for strained Si are given. The results indicate the need for accurate band-structure models to study strained devices. The non-equilibrium Green's function formalism provides a self-consistent approach for the analysis of nanoscale devices. In this formalism scattering processes and quantum mechanical phenomena can be rigorously modeled. We investigated the effect of line-edge roughness on the electronic properties of GNRs. An atomistic tight-binding model, which captures the granularity of the simulation domain, has been used. The results indicate the importance of employing non-continuum quantum mechanical simulations for the accurate analysis of nanoscale devices.

References

[1] International Technology Roadmap for Semiconductors - 2009 Edition, `http://public.itrs.net`.
[2] S. Selberherr, *Analysis and Simulation of Semiconductor Devices* (Springer-Verlag, Vienna, 1984).
[3] M. Lundstrom, *Fundamentals of Carrier Transport*, 2nd ed. (Cambridge University Press, Cambridge, 2000).
[4] C. Jacoboni *et al.*, *The Monte Carlo Method for Semiconductor Device Simulation* (Springer, Vienna, 1989).
[5] N. Goldsman *et al.*, Superlattices Microstruct. **27**, 159 (2000).
[6] C. Jungemann *et al.*, *Hierarchical Device Simulation* (Springer, Vienna, 2003).
[7] T. Grasser *et al.*, Proc. IEEE **91**, 251 (2003).
[8] C. Canali *et al.*, Phys. Rev. B **12**, 2265 (1975).
[9] C. Jacoboni *et al.*, J. Phys. Chem. Solids **36**, 1129 (1975).
[10] M. V. Fischetti *et al.*, Phys. Rev. B **38**, 9721 (1988).
[11] M. Fischetti *et al.*, in *26th European Solid State Device Research Conference*, 813 (1996)edited by G. Baccarani *et al.*
[12] M. V. Fischetti *et al.*, J. Appl. Phys. **94**, 1079 (2003).
[13] C. Jungemann *et al.*, *Hierarchical Device Simulation. The Monte Carlo Perspective* (Springer, 2003).
[14] C. S. Smith, Phys. Rev. **94**, 42 (1954).
[15] E. Ungersboeck *et al.*, IEEE Trans. Electron Devices **54**, 2183 (2007).
[16] V. Sverdlov *et al.*, in *Proc. EUROSOI 2007* 39 (January, 2007)
[17] R. Lake *et al.*, J. Appl. Phys. **81**, 7845 (1997).
[18] M. P. Anantram *et al.*, IEEE Trans. Electron Devices **54**, 2100 (2007).
[19] W. Tian *et al.*, J. Chem. Phys **109**, 2874 (1998).
[20] P. S. Damle *et al.*, Phys. Rev. B **64**, 201403 (2001).
[21] A. W. Ghosh *et al.*, Nano Lett. **4**, 565 (2004).
[22] A. Svizhenko *et al.*, J. Appl. Phys. **91**, 2343 (2002).
[23] R. Venugopal *et al.*, J. Appl. Phys. **93**, 5613 (2003).
[24] C. Rivas *et al.*, Phys. Status Solidi B **239**, 94 (2003).
[25] A. Svizhenko *et al.*, IEEE Trans. Electron Devices **50**, 1459 (2003).
[26] X. Shao *et al.*, Solid-State Electron. **49**, 1435 (2005).
[27] A. Martinez *et al.*, Physica E **37**, 168 (2006).
[28] M. Shin, IEEE Trans. Nanotechnol. **6**, 230 (2007).
[29] M. Luisier *et al.*, Phys. Rev. B **80**, 155430 (11pp) (2009).
[30] D. A. Stewart *et al.*, Phys. Rev. Lett. **93**, 107401 (2004).
[31] A. Svizhenko *et al.*, Phys. Rev. B **72**, 085430 (2005).
[32] L. Castro *et al.*, IEEE Trans. Nanotechnol. **4**, 699 (2005).
[33] M. Pourfath *et al.*, Nanotechnology **18**, 424036 (2007).
[34] S. O. Koswatta *et al.*, IEEE Trans. Electron Devices **54**, 2339 (2007).
[35] B. Obradovic *et al.*, Appl. Phys. Lett. **88**, 142102 (3pp) (2006).
[36] Y. Yoon *et al.*, Appl. Phys. Lett. **91**, 073103 (3pp) (2007).
[37] G. Fiori *et al.*, IEEE Electron Device Lett. **28**, 760 (2007).
[38] Y. Ouyang *et al.*, Appl. Phys. Lett. **92**, 243124 (3pp) (2008).
[39] Y. Sandu *et al.*, Phys. Rev. B **73**, 075313 (8pp) (2006).
[40] J. Guo *et al.*, Appl. Phys. Lett. **92**, 163109 (3pp) (2008).
[41] T. Low *et al.*, J. Appl. Phys. **104**, 094511 (10pp) (2008).
[42] L. V. Keldysh, Soviet Phys. JETP **20**, 1018 (1965).
[43] G. D. Mahan, Physics Reports **145**, 251 (1987).
[44] E. Wigner, Phys. Rev. **40**, 749 (1932).
[45] M. Nedjalkov *et al.*, Phys. Rev. B **70**, 115319 (16pp) (2004).
[46] R. K. Mains *et al.*, J. Appl. Phys. **64**, 5041 (1988).
[47] K. L. Jensen *et al.*, J. Appl. Phys. **67**, 7602 (1990).
[48] S. Datta, *Electronic Transport in Mesoscopic Systems* (Cambridge University Press, New York, 1995).
[49] H. Tsuchiya *et al.*, IEICE Trans. Electron. **E82-C**, 880 (1999).
[50] A. Geim *et al.*, Nature Mater. **6**, 183 (2007).
[51] K. Bolotin *et al.*, Solid-State Commun. **146**, 351 (2008).
[52] Y.-M. Lin *et al.*, Science **327**, 661 (2010).
[53] F. Xia *et al.*, Nano Lett. **10**, 715 (2010).
[54] C. Berger *et al.*, Science **312**, 1191 (2006).
[55] M. Han *et al.*, Phys. Rev. Lett. **98**, 206805 (4pp) (2007).
[56] T. Fang *et al.*, Phys. Rev. B **78**, 205403 (8pp) (2008).
[57] S. M. Goodnick *et al.*, Phys. Rev. B **33**, 8171 (1985).